Available online at www.sciencedirect.com
ScienceDirect
Geochimica et Cosmochimica Acta 71 (2007) 3656–3671
Geochimica et Cosmochimica Acta
www.elsevier.com/locate/gca

The origin of geochemical diversity of lunar mantle sources inferred from the combined U–Pb, Rb–Sr, and Sm–Nd isotope systematics of mare basalt 10017

Amy M. Gaffney [a,*], Lars E. Borg [a,1], Yemane Asmerom [b]

[a] Institute of Meteoritics, University of New Mexico, Albuquerque, NM 87131, USA
[b] Department of Earth and Planetary Sciences, University of New Mexico, Albuquerque, NM 87131, USA

Received 20 April 2006; accepted in revised form 4 May 2007; available online 17 May 2007

Abstract

The results of our combined U–Pb, Rb–Sr, and Sm–Nd isotope study of mare basalt 10017 contribute to the understanding of the petrogenetic processes involved in the origin of geochemical diversity in lunar mare basalt sources, as well as the U–Pb isotope systematics of the Moon. The Rb–Sr, Sm–Nd, and ^{238}U–^{206}Pb isotope systems yield concordant crystallization ages of 3.633 ± 0.057 Ga, 3.678 ± 0.069 Ga, and 3.616 ± 0.098 Ga, respectively. The ^{235}U–^{207}Pb isochron yields an older, though still concordant, age of 3.80 ± 0.12 Ga. Neither the ^{206}Pb–^{207}Pb system nor U–Pb concordia system yields an age for 10017 that is concordant with the age determined from the Sm–Nd, Rb–Sr, and ^{238}U–^{206}Pb systems. The initial $^{87}Sr/^{86}Sr$ of 10017 is 0.69941 ± 7 and the initial ε_{Nd} is $+3.2 \pm 0.4$. Initial Pb isotopic compositions, determined from the U–Pb isochrons, are $^{206}Pb/^{204}Pb_i = 31 \pm 11$ and $^{207}Pb/^{204}Pb_i = 34 \pm 15$. Together, these initial Pb compositions constrain the μ value of the 10017 source to be 70 ± 30, assuming a single-stage Pb growth model. This is considerably lower than μ values typically estimated for mare basalt sources (~100–600). Regardless, the μ values calculated for the sources of mare basalts, as well as other lunar samples, show a range that is larger than can be explained by fractionation of U from Pb solely by crystallization of silicate phases and ilmenite during magma ocean solidification and formation of lunar mantle sources. The U–Pb isotope systematics may reflect late-stage formation of a sulfide phase, which strongly fractionates Pb from U but has minimal effect on Rb/Sr or Sm/Nd compositions, during crystallization of the lunar magma ocean.

1. INTRODUCTION

Lunar mantle sources have the highest and apparently most variable μ ($^{238}U/^{204}Pb$) values determined for any terrestrial planetary body (e.g., Stacey and Kramers, 1975; Nyquist and Shih, 1992; Borg et al., 2005; Gaffney et al., 2006). Thus, a detailed understanding of these distinctive U–Pb isotope systematics has the potential to offer insights into issues such as elemental fractionation during magma ocean solidification and the degree of volatile depletion in the Moon. Because of both the volatile and chalcophile nature of Pb, the U–Pb isotope system may record evidence of these petrogenetic processes that is not preserved in Rb–Sr, Sm–Nd or Lu–Hf isotope systems. However, results of studies on lunar U–Pb isotope systematics are difficult to interpret because of the low abundance and very radiogenic nature of lunar Pb, as well as disturbance to lunar U–Pb isotope systems by impact processes and terrestrial Pb contamination during sample handling and analysis (e.g., Tatsumoto, 1970; Tera and Wasserburg, 1972). Extracting useful petrogenetic, as opposed to geochronologic, infor-

* Corresponding author. Present address: Lawrence Livermore National Laboratory, Chemistry, Material and Life Sciences Directorate, 7000 East Avenue, L-231, Livermore, CA 94550, USA. Fax: +1 925 422 3160.
E-mail address: gaffney1@llnl.gov (A.M. Gaffney).
[1] Present address: Lawrence Livermore National Laboratory, Chemistry, Material and Life Sciences Directorate, 7000 East Avenue, L-231, Livermore, CA 94550, USA.

0016-7037/$ - see front matter © 2007 Elsevier Ltd. All rights reserved.
doi:10.1016/j.gca.2007.05.005

mation from the U–Pb isotope system in lunar samples requires the ability to confidently establish the initial Pb isotopic composition from an isochron, and with this information, to determine the long-term μ value of the mantle source from which the sample originated.

Most Pb isotope studies of lunar samples rely on ^{206}Pb–^{207}Pb isochrons or U–Pb concordia to constrain ages. These data representations are favored because they do not require precise measurements of ^{204}Pb, which is the least abundant of the Pb isotopes and therefore the most susceptible to contamination and poor analytical precision. However, the drawback of these diagrams is that they do not directly provide the initial Pb isotopic composition of the sample, that is, the Pb isotopic composition of the magma at the time of crystallization. In order to infer an initial Pb isotopic composition from a Pb–Pb isochron or a U–Pb concordia diagram, a model history for Pb isotopic growth in the sample's mantle source prior to melt extraction must be assumed. In contrast, initial Pb isotopic compositions can be determined directly from $^{238}U/^{204}Pb$–$^{206}Pb/^{204}Pb$ and $^{235}U/^{204}Pb$–$^{207}Pb/^{204}Pb$ isochrons for undisturbed samples, provided that the ^{204}Pb abundance can be measured precisely. Current analytical capabilities have enabled significantly decreased total procedural laboratory Pb blanks, on the order of 10s of picograms, and analytical technology has advanced to allow the use of ion counters to measure the very low abundance ^{204}Pb mass. Together these advances provide the means to determine the ^{204}Pb abundance in lunar samples more precisely than what has been possible in the past. With precise measurements of ^{204}Pb, data can be represented as $^{238}U/^{204}Pb$–$^{206}Pb/^{204}Pb$ and $^{235}U/^{204}Pb$–$^{207}Pb/^{204}Pb$ isochrons which, for some samples, enable confident determination of initial Pb isotopic compositions.

This combined U–Pb, Rb–Sr, and Sm–Nd isotopic study of mare basalt 10017 contributes to the understanding of petrogenetic processes involved in the origin of geochemical diversity in mare basalt source regions, as well as the U–Pb systematics of the Moon. Our approach was to measure all three isotope systems on the same mineral and whole rock fractions, and to examine the U–Pb isotope systematics in the context of crystallization ages determined with more robust Sm–Nd and Rb–Sr isotope systems. In this study we: (1) define the crystallization age for 10017 using Rb–Sr, Sm–Nd, and U–Pb isotope systems, (2) describe the disturbance apparent in the U–Pb isotope systems and evaluate possible explanations for this disturbance, (3) determine the μ value of the 10017 mantle source, and (4) discuss the nature and origin of U/Pb heterogeneity in lunar mantle source regions.

2. ANALYTICAL PROCEDURES

2.1. Sample description

The sample chosen for this study, 10017,328, is a high-Ti, high-K mare basalt collected during the Apollo 11 mission. It contains 45–55% clinopyroxene (0.04–0.12 mm), 24–35% plagioclase (0.2–2.0 mm), 15–20% ilmenite (0.03–0.1 mm) and ~8% mesostasis (Schmitt et al., 1970; Apollo 11 Lunar Sample Catalogue, 1977; Beaty and Albee, 1978). Trace phases include cristobalite, tridymite, troilite, apatite, whitlockite, ulvöspinel, and Fe-metal (Papike et al., 1976; Beaty and Albee, 1978). Ilmenite is lath-like, skeletal and sieve-textured (Apollo 11 Lunar Sample Catalogue, 1977). Given the range in crystal size and mineralogical mode published for this sample, it is unlikely that the small sub-sample used for this study is truly representative of the entire specimen. Although this is not critical to the construction of isochron diagrams and their use for determining ages and initial isotopic compositions of 10017, this does suggest the possibility that the mineral and whole rock fractions analyzed do not completely account for possible chemical heterogeneity in this sample. For example, 10017 contains relatively abundant mesostasis, and heterogeneous distribution of this component throughout the rock would result in different isotopic and trace element compositions for different whole rock sub-samples. The sample chip used in this study is a piece left over from an experimental shock study undertaken by F. Hörz (personal communication; Nyquist et al., 1987). Although this chip had been drilled during preparation for the shock experiment, we took special care to exclude from our study any pieces that had been in contact with the drill bit surface. As discussed in the following sections, we do not observe any effects in the isotope systematics that can be consistently explained by contamination related to drilling.

2.2. Analytical techniques

A 739 mg aliquot of 10017,328 was crushed in a sapphire mortar and pestle and sieved in a stainless steel and nylon sieve set to 100–200 mesh (74–150 μm) and 200–325 mesh (44–74 μm) grain size fractions. Only the 100–200 mesh fraction was used for the mineral separates. A second chip was powdered and homogenized for bulk analyses. One ~10 mg sub-sample of this powder was spiked and used for the whole rock isotopic composition and concentration measurements. A second ~100 mg sub-sample was left unspiked and used to measure the Sm isotopic composition in order to evaluate the effects of neutron fluence on the sample. A Frantz isodynamic magnetic separator was used to make plagioclase-rich, pyroxene-rich, and ilmenite-rich mineral separates. This sample contains abundant oxide (assumed to be predominantly ilmenite) and mesostasis, and thus the plagioclase-rich and pyroxene-rich magnetic separates contained significant amounts of these additional components. Plagioclase-rich and pyroxene-rich magnetic separates were purified by hand-picking to remove grains containing oxide inclusions or other silicate mineral impurities. Approximately 60% of the plagioclase magnetic separate was rejected during hand-picking and ~90% of the pyroxene fraction was rejected during hand-picking. The purified plagioclase and pyroxene fractions are visually estimated to contain 99% plagioclase and 95% pyroxene, respectively. The Plag-rej and Px-rej mineral fractions comprise grains rejected during hand-picking of the plagioclase-rich and pyroxene-rich magnetic separates, respectively, and contain abundant oxide inclusions, composite grains and mesostasis. We visually estimate that the Plag-rej fraction contains 95% plagioclase, and that the Px-rej fraction

contains 75% pyroxene. It was impractical to further purify the ilmenite magnetic fraction with hand-picking. Ilmenite grains are small (30–100 μm), lath-like and sieve-textured, so there are very few pure ilmenite grains present in the ilmenite-rich magnetic fraction.

Mineral fractions were not further crushed after hand-picking. All fractions were cleaned with 0.5 N acetic acid for 10 min in an ultrasonic bath to remove Pb contamination on grain surfaces. This cleaning step was followed with a quartz-distilled water rinse. Special care was taken to not preferentially remove fine-grained material when pipetting liquid off the sample. The purified plagioclase and pyroxene fractions, as well as the whole rock fraction, were leached in 2 N HCl, for 10 min at room temperature in an ultrasonic bath. The leaching step was followed with a quartz-distilled water rinse. The HCl leachate and final water rinse for each sample were combined, processed, and analyzed for their isotopic composition. Residue mineral fractions that were leached are denoted with the suffix (R), and leachates with the suffix (L). Although the ilmenite fraction was washed in acetic acid, it was not treated to an HCl leaching step because ilmenite is soluble in this acid. The mineral separation procedure is shown schematically in Fig. 1.

After the acetic acid wash and HCl leaching (whole rock, purified plagioclase, and purified pyroxene fractions only), all mineral, whole rock, and leachate fractions were spiked with mixed Rb–Sr, Sm–Nd, and U–Pb isotopic tracers for elemental concentration measurements. Mineral fractions were digested with a combination of HCl, HF, and HNO_3. Uranium, Pb, Rb, Sr, Sm, and Nd were separated sequentially from these digestions and leachates following the procedures described by Borg et al. (2005). Procedural blanks were: $U = 4 \pm 3$ pg, $Pb = 12 \pm 6$ pg, $Rb = 6 \pm 4$ pg, $Sr = 11 \pm 4$ pg, $Sm = 5 \pm 3$ pg, and $Nd = 9 \pm 3$ pg (1 sigma). These values do not include blank contributions associated with the tracers, because the amounts of tracer solution used varied from fraction to fraction. The Rb–Sr and Sm–Nd tracer solutions were prepared from stock solutions from which Pb had been removed with ion exchange techniques. Additional Pb blank associated with tracer solutions ranges from 7 to 87 pg Pb. The data reported in Tables 1–3 have been corrected for procedural blank as well as blank associated with the tracer solutions. Isotopic analyses were conducted using a Micromass (VG) Sector 54 mass spectrometer at the University of New Mexico. Details on mass spectrometry are presented by Borg et al. (2005). Analytical results are shown in Tables 1–3.

3. RESULTS—ISOCHRONS AND AGES

3.1. Sm–Nd isochron

The Sm–Nd isochron age for 10017 is 3.633 ± 0.057 Ga (Fig. 2). This age is calculated from the six mineral and whole rock fractions analyzed: Plag(R), Plag-rej, Px(R), Px-rej, Ilm, and WR(R). The low MSWD (0.55) indicates a good fit of the isochron to the data. This isochron gives an initial ε_{Nd} of 3.2 ± 0.4, calculated using the method of Fletcher and Rosman (1982). ε_{Nd} notation describes deviation of the sample $^{143}Nd/^{144}Nd$ value from the chondritic value at the time of interest (time of crystallization, in this context), in parts per 10^4. This is consistent with the initial ε_{Nd} of 3.1 ± 0.4 determined from a single whole rock analysis of 10017, assuming an age of 3.59 Ga (Snyder et al., 1994). The three leachates have similar and relatively unradiogenic compositions, and fall very close to the isochron regressed through the mineral fractions. The age calculated for all analyzed fractions (purified minerals, rejects, whole rock and leachates) is 3.65 ± 0.10 Ga

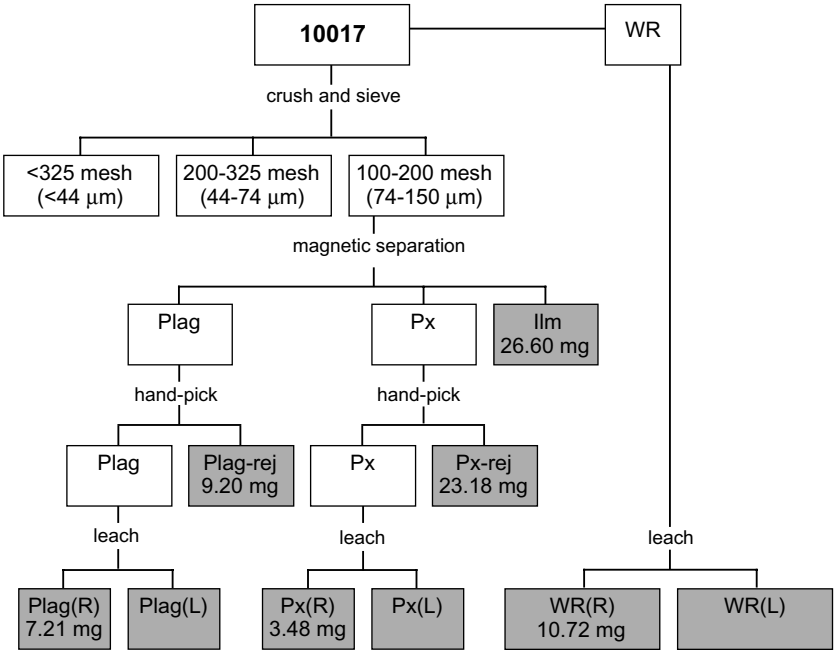

Fig. 1. Mineral separation scheme for 10017. Shaded boxes indicate analyzed fractions.

Table 1
Sm–Nd isotopic compositions of 10017

Fraction	wt. (mg)	Sm (ppm)	Sm (ng)	Nd (ppm)	Nd (ng)	$^{147}Sm/^{144}Nd$[a]	$^{143}Nd/^{144}Nd$[b]
Plag (R)	7.21	0.797	5.74	2.906	20.95	0.16575 ± 0.00017	0.512064 ± 0.000010
Plag (L)			0.88		2.83	0.18894 ± 0.00082	0.512648 ± 0.000012
Plag rej	9.20	1.686	15.51	5.226	48.08	0.19503 ± 0.00020	0.512765 ± 0.000010
Px (R)	3.48	6.48	22.53	13.256	46.13	0.29531 ± 0.00030	0.515167 ± 0.000010
Px (L)			6.68		21.31	0.18938 ± 0.00019	0.512553 ± 0.000010
Px rej	23.18	6.60	152.99	16.858	390.77	0.23668 ± 0.00024	0.513759 ± 0.000010
Wr (R)	10.72	6.228	66.77	15.108	161.95	0.24923 ± 0.00025	0.514094 ± 0.000010
Wr (L)			74.37		232.00	0.19380 ± 0.00019	0.512703 ± 0.000010
Ilm	26.60	45.2	1203.1	137.8	3665.7	0.19842 ± 0.00020	0.512836 ± 0.000010
La Jolla ($n = 3$)[c]					10		0.511869 ± 0.000040

Plag, plagioclase; Px, pyroxene; Wr, whole rock; Ilm, ilmenite; (L), HCl leachate; (R), residue of HCl leachate; rej, portion of mineral fraction rejected after hand-picking. All samples and standards run as NdO+.

Isochrons are calculated using either $2\sigma_p$ (from standard runs) or $2\sigma_m$ (from measured isotope ratios), whichever is larger.

[a] Error limits include a minimum uncertainty of 0.5% plus 50% of the blank correction for Sm and Nd added quadratically.

[b] Normalized to $^{146}Nd/^{144}Nd = 0.7219$. Uncertainties are $2\sigma_m$ calculated from the measured isotope ratios. $2\sigma_m = [\sum(m_i - \mu)^2/(n(n-1))]^{1/2}$ for n ratio measurements m_i with mean value μ.

[c] Error limits are $2\sigma_p$. $2\sigma_p = [\sum(M_i - \pi)^2/(N-1)]^{1/2}$ for N measurements M_i with mean value π.

Table 2
Rb–Sr isotopic compositions of 10017

Fraction	wt. (mg)	Rb (ppm)	Rb (ng)	Sr (ppm)	Sr (ng)	$^{87}Rb/^{86}Sr$[a]	$^{87}Sr/^{86}Sr$[b]
Plag (R)	7.21	0.483	3.48	511.4	3687	0.00273 ± 0.00003	0.699591 ± 0.000011
Plag (L)			0.026		6.4	0.0120 ± 0.0014	0.700265 ± 0.000010
Plag rej	9.20	0.715	6.57	471.4	4337	0.00439 ± 0.00004	0.699658 ± 0.000010
Px (R)	3.48	1.32	4.6	121.20	422	0.03155 ± 0.00032	0.701029 ± 0.000010
Px (L)			0.034		7.4	0.0133 ± 0.0012	0.700678 ± 0.000010
Px rej	23.18	1.690	39.18	209.2	4850	0.02337 ± 0.00023	0.700645 ± 0.000010
Wr (R)	10.72	4.47	47.91	122.10	1309	0.1059 ± 0.0011	0.704768 ± 0.000010
Wr (L)			0.43		287	0.00435 ± 0.00004	0.699871 ± 0.000011
Ilm	26.60	16.53	439.63	182.4	4851	0.2622 ± 0.0026	0.713315 ± 0.000010
NBS 987 ($n = 7$)[c]					500		0.710257 ± 0.000030

Plag, plagioclase; Px, pyroxene; Wr, whole rock; Ilm, ilmenite; (L), HCl leachate; (R), residue of HCl leachate; rej, portion of mineral fraction rejected after hand-picking.

Isochrons are calculated using either $2\sigma_p$ (from standard runs) or $2\sigma_m$ (from measured isotope ratios), whichever is larger.

[a] Error limits include a minimum uncertainty of 0.5% plus 50% of the blank correction for Rb and Sr added quadratically.

[b] Normalized to $^{86}Sr/^{88}Sr = 0.1194$. Uncertainties are $2\sigma_m$ calculated from the measured isotope ratios. $2\sigma_m = [\sum(m_i - \mu)^2/(n(n-1))]^{1/2}$ for n ratio measurements m_i with mean value μ.

[c] Error limits are $2\sigma_p$. $2\sigma_p = [\sum(M_i - \pi)^2/(N\text{-}1)]^{1/2}$ for N measurements M_i with mean value π.

(MSWD = 2.6), nearly identical to the age determined from the purified mineral and reject fractions alone, and consistent with the observation that the leachates fall close to or on the isochron. The small uncertainty on the calculated age, the concordance of this age with previously determined ages for this sample (discussed in Section 3.2), the fact that all mineral (purified and reject) and whole rock fractions define this isochron, the observation that the $^{147}Sm/^{144}Nd$ ratios of the purest mineral fractions and whole rock are distributed along the isochron in an order that is consistent with igneous crystallization, and that the leachates do not show significant scatter from the isochron, indicate that the Sm–Nd systematics in this sample most likely define its crystallization age and that this isotope system has not suffered significant disturbance since crystallization. Furthermore, the amounts of Nd in the fractions were large (ranging from 3 ng to 3.7 μg), so blank corrections were trivial and internal precision for mass spectrometry was excellent.

The leachates contain a significant fraction of the total rare earth element (REE) budget for the sample. The WR(L) fraction contains 53% of the total Sm and 59% of the total Nd. These large proportions are not the result of inadvertent incorporation of fine-grained rock powder into the leachate during decanting of the leachate because: (1) visual inspection indicated that only a minimal amount (micrograms) of fine-grained powder was present in the decanted leachate, (2) the acid used for leaching was 2 N HCl, which is not strong enough to dissolve the small amount of fine-grained material remaining in the leachate at room temperature and during the short times (minutes) involved, and (3) all solutions were centrifuged prior to loading on ion exchange columns to separate any insoluble residue from the sample solution. The large abundance of

Table 3
U–Pb isotopic compositions of 10017

Fraction	wt. (mg)	U (ppm)	U (ng)	Pb (ppm)	Pb (ng)	$^{238}U/^{204}Pb$[a]	$^{206}Pb/^{204}Pb$[b]	$^{207}Pb/^{204}Pb$[b]	$^{208}Pb/^{204}Pb$[b]
Plag (R)	6.48	0.024	0.155	0.102	0.662	42.1 ± 3.2	69.5 ± 2.0	58.3 ± 1.7	79.5 ± 1.7
Plag (L)			0.025		1.308	1.30 ± 0.14	20.624 ± 0.029	17.549 ± 0.030	40.974 ± 0.073
Plag rej	8.18	0.06	0.520	0.306	2.499	26.70 ± 0.67	47.47 ± 0.36	35.17 ± 0.24	64.78 ± 0.37
Px (R)	3.12	0.21	0.658	0.371	1.159	205.1 ± 2.4	175.11 ± 0.88	82.58 ± 0.43	159.92 ± 0.83
Px (L)			0.097		0.767	17.16 ± 0.70	43.00 ± 0.23	32.83 ± 0.16	80.52 ± 0.42
Px rej	20.49	0.24	4.919	0.603	12.359	115.2 ± 1.0	123.05 ± 0.20	72.48 ± 0.14	138.60 ± 0.30
Wr (R)	8.47	0.55	4.697	0.844	7.151	741.3 ± 6.5	590.3 ± 2.1	257.39 ± 0.96	459.4 ± 1.8
Wr (L)			1.438		3.279	115.8 ± 1.6	89.98 ± 0.98	49.85 ± 0.53	164.7 ± 1.8
Ilm	26.6	2.4	62.727	3.98	105.993	721.3 ± 3.1	573.79 ± 0.92	248.52 ± 0.45	588.6 ± 1.2
All Faraday runs: NBS 981 ($n = 10$)[c]					2		16.902 ± 0.034	15.440 ± 0.038	36.54 ± 0.11
Faraday-Daly runs: NBS 981 ($n = 17$)[c]					0.5–2		16.889 ± 0.081	15.436 ± 0.091	36.53 ± 0.24

Plag, plagioclase; Px, pyroxene; Wr, whole rock; Ilm, ilmenite; (L), HCl leachate; (R), residue of HCl leachate; rej, portion of mineral fraction rejected after hand-picking.

Isochrons are calculated using either $2\sigma_p$ (from standard runs) or $2\sigma_m$ (from measured isotope ratios), whichever is larger.

[a] Error limits include a minimum uncertainty of 0.5% plus 50% of the blank correction for U and Pb added quadratically.

[b] Uncertainties are $2\sigma_m$ calculated from the measured isotope ratios. $2\sigma_m = [\sum(m_i - \mu)^2/(n(n\text{-}1))]^{1/2}$ for n ratio measurements m_i with mean value μ.

[c] Error limits are $2\sigma_p$. $2\sigma_p = [\sum(M_i - \pi)^2/(N\text{-}1)]^{1/2}$ for N measurements M_i with mean value π. The greater uncertainty on the Faraday-Daly standard runs reflects the added uncertainty from the Faraday-Daly gain calibration.

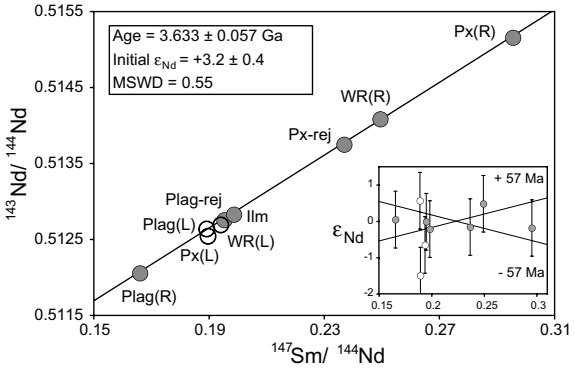

Fig. 2. $^{147}Sm/^{144}Nd$–$^{143}Nd/^{144}Nd$ isochron for 10017. All analyzed fractions are shown in the plot. All mineral and whole rock fractions (gray symbols) are used in the age calculation; leachates (open symbols) are not used in the age calculation. Age was calculated using Isoplot/Ex rev 2.49 (Ludwig, 2001). Initial ε_{Nd} calculated using method of Fletcher and Rosman (1982). Inset shows deviation of individual fractions from the isochron, in epsilon units. Analytical uncertainty is smaller than symbol size, or otherwise as shown.

Sm and Nd in the leachate as well as the proximity of the leachate compositions to the isochron suggest that the leachates are dominated by primary igneous phosphates. The high abundances of REE in phosphates and the control of Sm–Nd isotope systematics in leachates by dissolved phosphates has been well documented in the lunar and martian literature (e.g., Jolliff et al., 1993; Borg et al., 1997, 2003). The compositions of the leachates are similar to those of the Plag-rej and Ilm fractions, both of which are unleached, again indicating that the phosphates have a large control on the REE budget in this sample. Only one of the three leachates (Px(L)) falls below and outside of uncertainty of the isochron. This may represent a minor disturbance to the phosphates or REE on grain boundaries and surfaces.

The isotopic composition of lunar samples can be modified through capture of thermal neutrons generated by spallation reactions resulting from bombardment of the lunar surface by high-energy cosmic radiation. The total thermal neutron fluence that a sample experiences is a function of the integrated time-depth history of the sample's residence in the lunar crust, the composition (density) of surrounding material (which can shield the sample from thermal neutrons), and fluctuations in intensity of cosmic radiation over time. Apollo 15 and 17 drill cores, which extend to depths of 500 g/cm^2 (reported as g/cm^2 to account for varying density of material throughout the core; 535 g/cm^2 corresponds to an absolute depth of 289 cm in the Apollo 17 core, Curtis and Wasserburg, 1975), show measurable neutron fluences, as monitored with ^{149}Sm, ^{155}Gd, and ^{157}Gd, over their entire lengths (Russ et al., 1972; Curtis and Wasserburg, 1975; Hidaka et al., 2000). Of concern to our study are the potential effects of thermal neutron capture on the Sm and Nd isotopic composition of 10017.

Samarium-149 has a very large thermal neutron capture cross section (4×10^{-24} m^2), orders of magnitude larger than that of any of the other isotopes of Sm or Nd, so we use $^{149}Sm/^{152}Sm$ measured on an unspiked aliquot (~100 mg) of 10017 whole rock powder to monitor and correct for neutron fluence. It is particularly important to correct for the effect of thermal neutron fluence on ^{149}Sm because this is the principal (~98%) mass in the Sm spike. In order to accurately deconvolute the spiked sample data, it is necessary to know the isotopic composition of Sm in the sample; it is not appropriate to assume natural proportions in a sample that has experienced a significant neutron fluence. The measured $^{149}Sm/^{152}Sm$ for 10017 is 0.514753. This corresponds to $\varepsilon_{149Sm} = -40.75$, where ε_{149Sm} repre-

sents the deviation of $^{149}Sm/^{152}Sm$ in the sample from the natural ratio, in parts per 10^4. This ratio, as well as the correspondingly high measured $^{150}Sm/^{152}Sm$ (0.278176), are used as the actual sample Sm compositions in the spike deconvolution calculations for the Sm data. All other Sm isotopes are present in natural proportions.

The corrections on $^{143}Nd/^{144}Nd$ are minor, and are based on the measured $^{149}Sm/^{152}Sm$ value according to the relationship: $\Delta\varepsilon_{Nd} = 0.004 * \varepsilon_{149Sm}$ (Nyquist et al., 1995). This expression is a simplification of the algorithms of Lingenfelter et al. (1972), and has been shown to be a good approximation for lunar conditions (Nyquist et al., 1995). The corresponding absolute correction on the 10017 fractions is $\Delta^{143}Nd/^{144}Nd = -0.000008$, which is smaller than the analytical uncertainty.

3.2. Rb–Sr isochron

The best Rb–Sr age, calculated from five purified and reject mineral fractions, is 3.678 ± 0.069 Ga (MSWD = 4.8), with an initial $^{87}Sr/^{86}Sr$ of 0.69941 ± 0.00007 (Fig. 3). This age is concordant with the Sm–Nd age. The amounts of Sr analyzed in the 10017 fractions range from 400 ng to 5 μg; thus blank corrections and in-run statistics for mass spectrometry runs do not make a significant contribution to the analytical uncertainties (Table 2). Several studies have previously reported Rb–Sr ages and $^{87}Sr/^{86}Sr$ initials for 10017. These ages, corrected to $\lambda^{87}_{Rb} = 0.01402\ Ga^{-1}$ (Minster et al., 1982; Begemann et al., 2001) are: 3.56 ± 0.05 Ga (Papanastassiou et al., 1970), 3.54 ± 0.22 Ga (Gopalan et al., 1970), and 3.67 ± 0.07 Ga (Nyquist et al., 1987). Initial $^{87}Sr/^{86}Sr$ values include: 0.69942 ± 0.00002, calculated from a whole rock and an assumed crystallization age of 3.59 Ga (Snyder et al., 1994); 0.69942 ± 0.00006, calculated from an isochron (Papanastassiou et al., 1970); and 0.69931 ± 0.00007, also calculated from an isochron (Nyquist et al., 1987). The initial value cited above from the Caltech lab (Papanastassiou et al., 1970) has been adjusted to NBS 987 $^{87}Sr/^{86}Sr = 0.71025$, to be consistent with the standard values from the JSC (Nyquist et al., 1987), Michigan (Snyder et al., 1994) and UNM labs. Although our age agrees with the Caltech age only at the limits of uncertainty, there is a good agreement between our age and the JSC age. Our age is also in agreement with the UCLA age (Gopalan et al., 1970), in part because the quoted uncertainties on this age are so large. Although there is some variability in the initial $^{87}Sr/^{86}Sr$ values determined by the multiple labs, this is a function of variation in the corresponding crystallization ages. When considering the initial values at a common crystallization age, our value is within uncertainty of all other previously published initials, although scatter among the values is still evident.

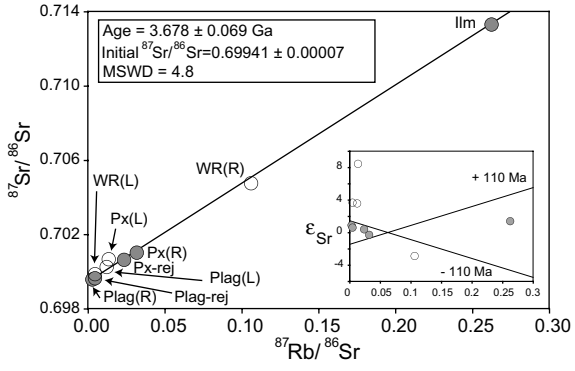

Fig. 3. $^{87}Rb/^{86}Sr$–$^{87}Sr/^{86}Sr$ isochron for 10017. All analyzed fractions are shown in the plot. Plag(R), Plag-rej, Px(R), Px-rej, and Ilm fractions (gray symbols) are used for the age calculation. Age was calculated using Isoplot/Ex rev 2.49 (Ludwig, 2001), and $\lambda^{87}_{Rb} = 0.01402\ Ga^{-1}$. Analytical uncertainty is smaller than symbol size. Inset shows deviation in epsilon units of individual fractions from the isochron calculated using all mineral and whole rock fractions (3.67 ± 0.11 Ga, initial $^{87}Sr/^{86}Sr = 0.69938 \pm 0.00017$, MSWD = 11.7).

The Rb–Sr age calculated using the same six fractions (WR(R) and all minerals) used for the Sm–Nd age is 3.67 ± 0.11 Ga (MSWD = 11.7), with an initial $^{87}Sr/^{86}Sr$ of 0.69938 ± 0.00017. Although this age and initial are within agreement of the best age and initial determined using only the mineral fractions, they have considerably larger uncertainties, introduced by the inclusion of the WR(R) fraction in the calculation. The WR(R) fraction is not within uncertainty of the 3.67 ± 0.11 Ga isochron, even though it was included in the calculation of the isochron (Fig. 3 inset). The whole rock fraction was leached as a powder, whereas the Plag(R) and Px(R) fractions were leached as fragments 74–150 μm in size, and the other fractions (Plag-rej, Px-rej, Ilm) were not leached at all, so the leaching may have more effectively removed a minor radiogenic component from the whole rock fraction than from the mineral fractions. However, the recombined WR fraction (R + L) also lies outside of uncertainty of the isochron (not shown), indicating that, regardless of leaching, the recombined WR fraction represents some post-crystallization disturbance of the sample that is not evident in any of the mineral separates.

The three leachate fractions fall outside of uncertainty of this isochron. In contrast to the Sm–Nd system, where the leachates lie very close to or within uncertainty of the isochron and have compositions that are controlled by primary igneous phosphates, the Rb–Sr isotopic compositions of the leachates reflect contamination or disturbance to the system. The observation that the leachates lie above the isochron defined by the mineral fractions may result from the loss of ^{87}Rb from mineral surfaces due to volatilization during a post-crystallization heating event. This would shift points to the left on the isochron diagram. In this case, the amount of ^{87}Rb mobilization is quite small, as the leachates contain <1% of the total Rb for each recombined (residue + leachate) fraction. Alternatively, this may simply indicate that the leaching step effectively removed a minor component of terrestrial Sr contamination, that was added to the sample during handling. However, even if there is a component of terrestrial contamination in the leachates, it is evident that it does not dominate the compositions, as this Sr is much less radiogenic than the least radiogenic terrestrial Sr ($^{87}Sr/^{86}Sr \sim 0.702$).

3.3. U–Pb isotope systematics

3.3.1. U–Pb isochron diagrams

The age calculated from the line regressed through all six mineral and whole rock fractions in the $^{238}U/^{204}Pb$–$^{206}Pb/^{204}Pb$ isochron diagram is 3.616 ± 0.098 Ga (MSWD = 86) and the initial $^{206}Pb/^{204}Pb$ is 31 ± 11 (Fig. 4a, Table 3). The age calculated from the line regressed through these same fractions on the $^{235}U/^{204}Pb$–$^{207}Pb/^{204}Pb$ isochron diagram is 3.78 ± 0.12 Ga (MSWD = 455) and the initial $^{207}Pb/^{204}Pb$ is 34 ± 15 (Fig. 4b). The amounts of Pb analyzed in these fractions range from ~650 pg to ~105 ng, and the sample-to-blank (procedural blank + spike blank) ratios range from ~7 to ~1300. The relatively high MSWD values for these ages may indicate, in part, that the analytical uncertainties are underestimated. However, more importantly, they may point to some degree of disturbance to the U–Pb isotope systematics, especially to the ^{235}U–^{207}Pb system, in which mineral fractions show greater scatter about the isochron than in the ^{238}U–^{206}Pb system. Regardless, both of these ages are within uncertainty of the ages determined from the Sm–Nd and Rb–Sr isochrons (Fig. 5) and thus the measured U–Pb isotope systematics must at least approximate the undisturbed igneous compositions.

The unradiogenic ends of the U–Pb isochrons are controlled by the plagioclase and pyroxene fractions. The Plag-rej and Px-rej fractions are both less radiogenic than their counterpart purified, leached mineral fractions, confirming that terrestrial contamination is still present in the unleached fractions and that the leaching step effectively removes some, and possibly most, of the terrestrial contamination. The radiogenic end of the isochron is defined by the WR(R) and Ilm fractions. Glass-rich mesostasis is a component that is common to both of these fractions, and likely controls their U/Pb ratios and Pb isotopic compositions. Because mesostasis is the very latest-stage crystallization product, it is very enriched in incompatible trace elements. Thus, a small amount of mesostasis can have a large effect on the incompatible trace element concentrations of a mineral or whole rock fraction. Conversely, ilmenite has very low partition coefficients for U and Pb, so pure ilmenite does not exert a significant control on the budgets of these elements in a sample. However, because ilmenite was a late-crystallizing phase in 10017, and the Ilm fraction was not purified by hand-picking, it is likely that the U–Pb composition of this fraction is actually controlled by the high incompatible element concentrations of mesostasis. The Ilm fraction was not leached, so it also contains a component of terrestrial Pb contamination. However, the Ilm fraction has a nearly identical composition to the leached WR(R) fraction, suggesting that terrestrial contamination does not make a significant contribution to the Pb isotopic budget of the Ilm fraction. Lastly, based on the relatively unradiogenic Pb composition of the WR(L) fraction compared to the very radiogenic WR(R) fraction, it is evident that leaching does not dissolve the glassy, high-μ mesostasis component. If phosphates have high U/Pb ratios, then the unradiogenic nature of Pb in the leachates suggest this phase contributes minimally to the Pb budget of the leachate.

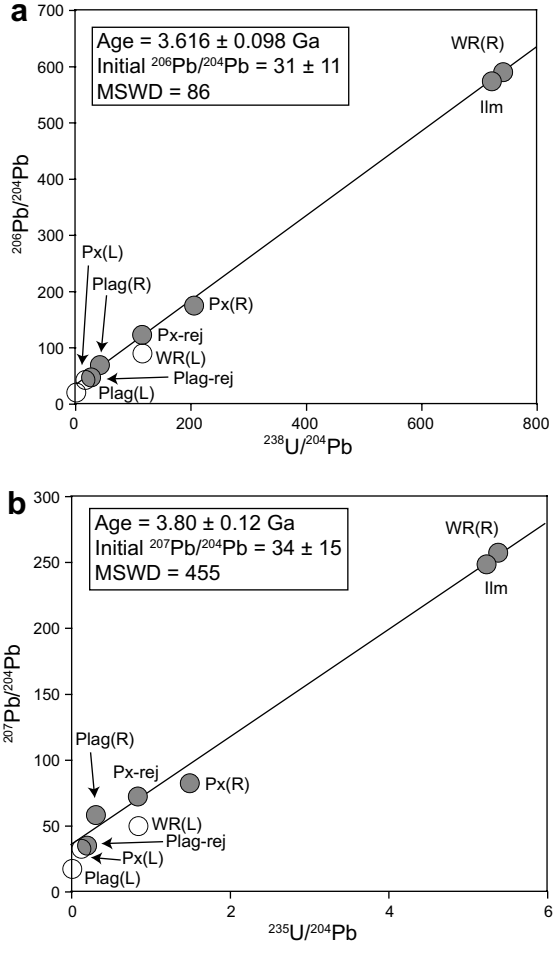

Fig. 4. (a) $^{238}U/^{204}Pb$–$^{206}Pb/^{204}Pb$, and (b) $^{235}U/^{204}Pb$–$^{207}Pb/^{204}Pb$ isochrons for 10017. All analyzed fractions are shown in the plot. All mineral fractions (gray symbols) are included in the age calculations for both isochrons. Ages are calculated using Isoplot/Ex rev 2.49 (Ludwig, 2001).

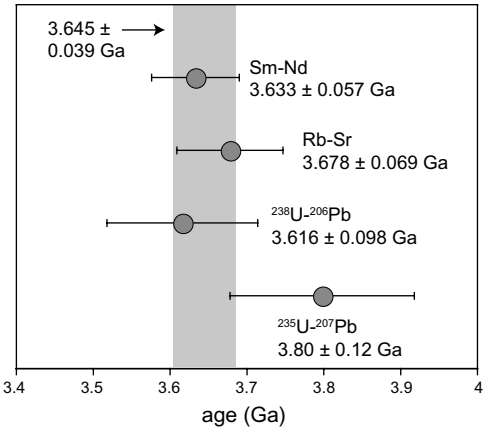

Fig. 5. Comparison of ages calculated for 10017, from isochrons shown in Figs. 2–4. Shaded field represents weighted average age calculated from Rb–Sr, Sm–Nd, and ^{238}U–^{206}Pb systems.

The leachates contain a significant proportion of the Pb and U in the sample: 30–60% of the total Pb for each mineral or whole rock fraction, relative to reconstructed abundances (leached residue + leachate) and 13–23% of the total U. The leachates contain a combination of Pb derived from both terrestrial and lunar sources. The leaching step is designed to remove terrestrial contamination, and it accomplishes this, as evident in the observation that the leachates are generally the least radiogenic fractions analyzed. However, although the leachates are unradiogenic relative to the rest of the fractions, they are more radiogenic than terrestrial Pb, indicating that the leachates also contain lunar Pb. There are several ways that lunar Pb may be incorporated into the leachates; lead-rich soluble phases (e.g., sulfides) may be dissolved in the leachate, the leachate may remove lunar-derived contamination that adhered to grain surfaces, or leaching may sample Pb that has diffused to grain boundaries during minor thermal metamorphism. The fact that all the leachates, leached residues and unleached fractions fall close to the isochrons indicates that leaching does not generate significant U–Pb fractionation, regardless of the large amounts of Pb in the leachates.

Using the concordancy of ages determined from the ^{238}U–^{206}Pb and ^{235}U–^{207}Pb isochron diagrams with Sm–Nd and Rb–Sr ages as an indication that the U–Pb system in this sample preserves primary petrogenetic information, we use the initial $^{206}Pb/^{204}Pb$ and $^{207}Pb/^{204}Pb$ determined from these diagrams to constrain the μ value of the 10017 mantle source. Assuming single-stage Pb growth from 4.558 to 3.633 Ga, starting from the initial Pb composition of Canyon Diablo Troilite (Tatsumoto et al., 1973; Chen and Wasserburg, 1983), the μ value calculated from the initial $^{206}Pb/^{204}Pb$ is 80 ± 41. An analogous μ value of 61 ± 39 is calculated from the initial $^{207}Pb/^{204}Pb$. The range of μ values that satisfies constraints from both $^{206}Pb/^{204}Pb$ and $^{207}Pb/^{204}Pb$ initials is 70 ± 30.

Another reasonable framework in which to consider the mantle source history of 10017 is a two-stage model for Pb growth. The $^{206}Pb/^{204}Pb$ and $^{207}Pb/^{204}Pb$ initial values are also consistent with this model. In the context of the lunar magma ocean model, which is commonly used to explain many of the geochemical and petrologic features of lunar rocks (e.g., Smith et al., 1970; Wood et al., 1970; Warren, 1985), the first stage of Pb growth corresponds to the earliest stages of the Moon's history, during the time of the lunar magma ocean. The $^{238}U/^{204}Pb$ during this stage of growth, μ_1, is inferred to be the bulk μ value of the Moon. The second stage of Pb growth began when the magma ocean crystallized to form the various lunar mantle geochemical reservoirs. The second stage of Pb growth ended when the lunar mantle melted to give rise to the 10017 parent magma. The $^{238}U/^{204}Pb$ during this stage of growth, μ_2, is the μ value of the 10017 mantle source. We model the pairs of μ_1 and μ_2 that are consistent with this model. In this calculation, T_0 is 4.558 Ga, and the initial Pb isotopic composition is that of Canon Diablo Troilite. The calculation is repeated three times, using three possible values for t_1: 4.527 Ga (Hf–W age inferred for lunar magma ocean crystallization, Kleine et al., 2005), 4.42 Ga (KREEP model age, Nyquist and Shih, 1992), or 4.32 Ga (^{146}Sm–^{142}Nd closure age, Nyquist et al., 1995). t_2 is 3.633 Ga, the crystallization age determined from the Sm–Nd isochron. Permissible pairs of μ_1 and μ_2 are inversely correlated, and μ_1/μ_2 increases as t_1 increases. At $t_1 = 4.32$ Ga, $\mu_1 < 285$ and $\mu_2 < 150$; at $t_1 = 4.42$ Ga, $\mu_1 < 470$ and $\mu_2 < 125$; at $t_1 = 4.527$ Ga, $\mu_1 < 2000$ and $\mu_2 < 105$. The values listed here are all maxima. Because μ_1 and μ_2 are inversely correlated, if one μ value is at its maximum, then the other will be at its minimum (as low as 10, in these calculations). Estimates of lunar bulk μ values, based on low μ values measured in some anorthosites and primitive basalts (Premo et al., 1999), are much lower than those commonly estimated for mare basalt sources (e.g., Nyquist and Shih, 1992). Thus, assuming that $\mu_1 < \mu_2$, μ_1 is likely to be much lower than the maximum estimates calculated here. Regardless of the parameters used to calculate μ_2, the inferred source μ for 10017 is less than 150. However, this calculation does not place significant independent constraints on the bulk μ value of the Moon.

3.3.2. Pb–Pb diagram

Lead–lead plots, in both conventional format ($^{206}Pb/^{204}Pb$ vs. $^{207}Pb/^{204}Pb$) and Tera–Wasserburg (T–W) format ($^{204}Pb/^{206}Pb$ vs. $^{207}Pb/^{206}Pb$, Tera and Wasserburg, 1974) fail to yield coherent age information for this sample (Fig. 6). This indicates that Pb in this system has experienced some disturbance. On the T–W diagram (Fig. 6a), the six mineral and whole rock fractions do not define a single line. Even the best lines regressed through subsets of points yield ages with high uncertainties and MSWDs. The age determined from the line regressed through all six mineral fractions is 3.85 ± 0.66 Ga (MSWD = 1959). The fractions Plag(R), Px-rej, WR(R) and Ilm yield an age of 3.79 ± 0.39 Ga (MSWD = 135), and the fractions Plag-rej, Px(R), WR(R) and Ilm yield an age of 3.89 ± 0.20 Ga (MSWD = 386). Although the data appear more linear in the conventional Pb–Pb diagram (Fig. 6b) than in the T–W diagram, the conventional data representation also yields ages that are older than the Sm–Nd age and that have large uncertainties: the age determined from all six mineral fractions is 3.90 ± 0.13 Ga (MSWD = 1624), the fractions Plag(R), Px-rej, WR(R) and Ilm yield an age of 3.85 ± 0.12 Ga (MSWD = 107) and the fractions Plag-rej, Px(R), WR(R) and Ilm yield an age of 3.95 ± 0.091 (MSWD = 750).

In Pb–Pb compositional space, the WR(R) and Ilm fractions are not consistent with the combination of the 3.633 Ga crystallization age and the initial Pb isotopic composition determined from the U–Pb isochrons. These fractions fall above the 3.633 Ga reference isochron drawn in the conventional Pb–Pb plot to intersect the initial Pb composition (Fig. 6b). In the T–W Pb–Pb plot, the Ilm, and WR(R) fractions are proximal to the y-axis, and therefore should closely represent the composition of radiogenic Pb in the sample ($^{207}Pb/^{206}Pb = 0.33$ at 3.633 Ga). However, the $^{207}Pb/^{206}Pb$ in these fractions is higher, at 0.43. These observations indicate either that the Ilm and WR(R) fractions have been contaminated by Pb with very high $^{207}Pb/^{206}Pb$, or that the true initial $^{207}Pb/^{206}Pb$ for the sample is much higher than calculated from the U–Pb isochrons. These possibilities are discussed further in Section 4.

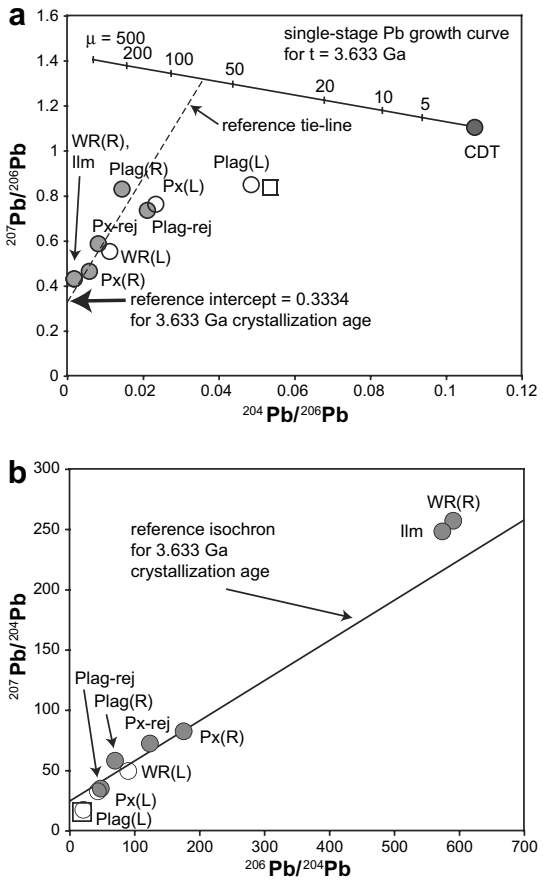

Fig. 6. (a) $^{204}Pb/^{206}Pb$–$^{207}Pb/^{206}Pb$ (Tera and Wasserburg, 1974), and (b) $^{206}Pb/^{204}Pb$–$^{207}Pb/^{204}Pb$ (conventional) Pb–Pb diagrams for 10017. All analyzed fractions are shown on these figures. Whole rock as well as pure mineral and reject fractions are shown with shaded symbols, and leachates are shown with open symbols. The composition of modern terrestrial Pb is shown with square symbol (Stacey and Kramers, 1975). (a) Large arrow indicates the reference radiogenic $^{207}Pb/^{206}Pb$ composition (y-intercept) for 3.633 Ga crystallization age; sub-horizontal line is the single-stage Pb growth curve at 3.633 Ga. Also shown is the reference tie-line between the initial Pb from a source with a μ value of 70 (on the single-stage Pb growth curve) and 3.633 billion year old radiogenic Pb. (b) Shown is the reference isochron for a 3.633 Ga crystallization age, drawn through initial $^{207}Pb/^{204}Pb$ and $^{206}Pb/^{204}Pb$ determined from U–Pb isochrons. Analytical uncertainty is smaller than symbol size.

3.3.3. U–Pb concordia

Uranium–lead concordia diagrams use proportions of radiogenic Pb in a sample to infer ages of major geologic events that resulted in U–Pb fractionation in a sample or its mantle source. The proportions of radiogenic Pb in a sample are calculated by subtracting the Pb initially present in the sample from the measured Pb isotopic compositions. In order to determine the appropriate composition of initial Pb for a sample, it is necessary to make some assumptions about its history. The traditional approach for lunar samples is to assume that the initial Pb is primordial, and therefore that the sample preserves a coherent history extending back to the formation of the Moon. This approach works reasonably well for ancient lunar samples that formed during initial differentiation of the Moon, but is less successful for younger mare basalts that formed during a subsequent episode of mantle melting. In principle, calculating radiogenic Pb isotopic compositions using the initial Pb incorporated into the basalt at the time of crystallization should yield the crystallization age on a concordia diagram.

Regardless of the chosen composition for initial Pb, 10017 fails to yield any age on a concordia diagram that is concordant with the crystallization age. Furthermore, we have identified no initial Pb composition that resulted in colinearity of more than four mineral or whole rock fractions. Using primordial Pb as the initial Pb composition, four fractions, WR(R), Ilm, Px(R) and Px-rej are reasonably colinear, and the upper and lower concordia intercepts derived from these four fractions correspond to ages of 4.324 ± 0.097 and 3.02 ± 0.29, respectively, with a MSWD of 4.5 (Fig. 7). The two plagioclase fractions lie above the concordia, in the field of 'unsupported Pb'. Using an initial Pb composition determined from the U–Pb isochrons yields results that are no more consistent with the known history of the sample. There is no combination of $^{206}Pb/^{204}Pb_i$ and $^{207}Pb/^{204}Pb_i$ within the uncertainties on these values determined from the U–Pb isochrons that results in colinearity of all six rock and mineral fractions on the concordia diagram, or results in any sub-set of values that define a line with an intercept that corresponds to an age that is concordant with the 10017 Rb–Sr and Sm–Nd crystallization age. From these observations, it is evident that the mineral fractions record a disturbance to their U–Pb systematics. The nature of the disturbance to the U–Pb system is discussed in detail below.

4. DISTURBANCE TO U–PB ISOTOPE SYSTEMATICS

As shown in the preceding discussion, it is possible for one Pb geochronologic system to yield coherent age information (U–Pb isochrons) where other Pb systems fail

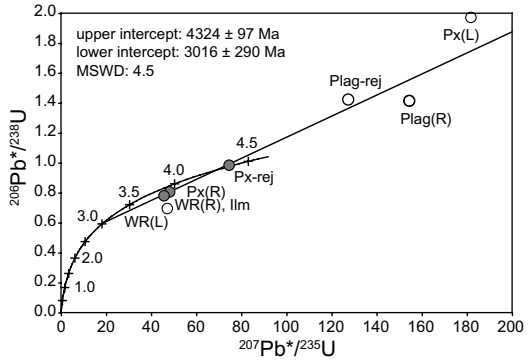

Fig. 7. Concordia diagram for 10017. All fractions are corrected for initial Pb with a primordial (CDT) composition. The four most colinear fractions, WR(R), Ilm, Px(R), and Px-rej are used in the calculation of intercept ages. The Plag(L) fraction falls off the scale of this figure, in the direction of very high $^{207}Pb^*/^{235}U$ and $^{206}Pb^*/^{238}U$. Numbered tick-marks on the concordia curve represent ages in Ga.

(Pb–Pb isochron, U–Pb concordia). This is also the case for a number of other lunar samples (e.g., Unruh and Tatsumoto, 1977; Premo and Tatsumoto, 1991; Edmunson et al., 2006). Thus, for any lunar sample, it is necessary to evaluate all U–Pb isotope data in the context of known Rb–Sr and Sm–Nd crystallization ages in order to extract useful petrogenetic information from the Pb isotope systematics. This is especially important because most, if not all, lunar samples show some disturbance to their U–Pb isotope systematics. Evidence for disturbance in 10017 includes: (1) a slightly older ^{235}U–^{207}Pb age compared to ^{238}U–^{206}Pb, Sm–Nd, and Rb–Sr ages; (2) best U–Pb concordia intercept ages that do not record the crystallization age; (3) Pb–Pb ages that are older than the Sm–Nd crystallization age, and have large uncertainties and MSWDs; and (4) non-colinearity of the mineral fractions in concordia and Pb–Pb compositional space. In the following section, we discuss possible mechanisms that could account for these observations of the U–Pb systematics of lunar samples. Simply stated, the possibilities are that the sample has lost or gained uranium, lead or both. We assume the crystallization age is that given by the concordant Sm–Nd and Rb–Sr isochron ages.

Two ways that disturbance to U might affect the daughter Pb isotope systems are, (1) differential loss of ^{222}Rn and ^{219}Rn, the gaseous intermediate daughter products in, respectively, the ^{238}U and ^{235}U decay chains, and (2) thermal neutron capture effects. The 10017 results are not consistent with the predicted effects for either of these mechanisms. Diffusional loss of Rn would have the effect of lowering the apparent ^{238}U–^{206}Pb age relative to the ^{235}U–^{207}Pb age, as well as lowering both of these ages relative to the crystallization age. However, the ^{235}U–^{207}Pb age is greater than the ^{238}U–^{206}Pb age, which in turn is concordant with the Rb–Sr and Sm–Nd ages. Therefore, this sample does not appear to have experienced Rn loss. The Sm isotopic composition of this sample indicates that it has experienced a large thermal neutron fluence, which has the potential to affect its U isotopic composition. However, given the thermal neutron capture crosssections of U, this mechanism is predicted to generate less than a 0.002% change in $^{238}U/^{235}U$. This is considerably lower than the analytical uncertainty on the U concentration measurements.

Disturbance to the Pb isotope systematics of 10017 may result from either loss or gain of Pb. Lead loss occurs through diffusion, which may be enhanced for radiogenic Pb that resides in lattice sites damaged by alpha particles released though radioactive decay of U. Because of the shorter half-life of ^{235}U relative to ^{238}U, the ratio of radiogenic ^{207}Pb to radiogenic ^{206}Pb, $^{207}Pb^*/^{206}Pb^*$, decreases continuously over time. Therefore, either continuous or instantaneous diffusional loss of radiogenic Pb at some time in the past would result in a Pb–Pb age that is younger than the actual crystallization age of the sample. However, the best Pb–Pb ages for 10017 are older than the crystallization age, indicating 10017 has not experienced significant diffusional Pb loss.

Lead contamination is another possible explanation for the disturbance of the U–Pb isotope systematics in 10017. This contamination may be either lunar or terrestrial in origin. The conventional Pb–Pb diagram illustrates the effects of contamination (Fig. 6a). A line corresponding to the 3.633 Ga crystallization age has a slope lower than that of the array defined by the mineral fractions. Thus, either the fractions at the unradiogenic end of the array (plagioclase and pyroxene) have $^{207}Pb/^{206}Pb$ compositions that are too low relative to the compositions of the Ilm and WR(R) fractions for a crystallization age of 3.633 Ga, or the fractions at the radiogenic end of the array (WR(R) and Ilm) have $^{207}Pb/^{206}Pb$ compositions that are too high relative to the plagioclase and pyroxene. Both of these possibilities are consistent with contamination. Terrestrial Pb preferentially added to plagioclase and pyroxene would lower $^{207}Pb/^{206}Pb$ in these fractions, whereas ancient Pb with high $^{207}Pb/^{206}Pb$ derived from the lunar surface preferentially added to the WR(R) and Ilm fractions would increase the $^{207}Pb/^{206}Pb$ in these fractions. Although both scenarios are possible, they are not equally probable.

Any terrestrial Pb contamination present in 10017 was acquired through the process of sample handling. Because the Pb blanks associated with chemical processing are very low and well known, it is unlikely that the data include significant unrecognized chemistry blank. Although the other steps of sample handling and processing, prior to the sample entering the clean lab for analysis, may have contributed terrestrial Pb contamination to the sample, this contamination is likely to be present only on grain surfaces in the sample. The sample has not been exposed to terrestrial Pb for long enough time under conditions that would facilitate diffusion of terrestrial Pb into the crystals. Furthermore, the unradiogenic compositions of the HCl leachates show that the leaching step effectively removes terrestrial Pb from the sample. Lastly, in order for terrestrial Pb contamination to be the principal cause of disturbance, it would require that terrestrial Pb preferentially contaminate the plagioclase and pyroxene fractions.

During its 3.633 billion year residence history on the surface of the Moon, 10017 has very likely had ample opportunity for contamination with ancient, high-207/206 Pb derived from the lunar surface. Lead may be volatilized and re-condensed with each meteorite impact event during the Moon's protracted bombardment history, and this is a geologic process through which 10017, or any other lunar sample, may gain lunar Pb contamination (e.g., Silver, 1970; Dickinson et al., 1989; Premo et al., 1999). This contamination is likely concentrated in the glassy mesostasis, which should be more susceptible than the crystalline components to Pb diffusion during periods of higher temperatures following impacts. Because this mesostasis is abundant in the WR(R) and Ilm fractions, and dominates their incompatible trace element signatures, these fractions show the largest effects of lunar Pb contamination. Additionally, all the leachates contain a lunar Pb component. On the other hand, the Plag(R) and Px(R) fractions have been purified by hand-picking specifically to remove mesostasis, so these fractions should have the lowest amounts of lunar Pb contamination of all the fractions, and most faithfully represent the true Pb isotopic composition and source μ value of 10017. This mechanism of contamination would

not affect the refractory REEs, so the Sm–Nd age is immune to this process. The Rb–Sr systematics of the leachates and the WR(R) fraction also show some evidence of Rb mobilization, as discussed in Section 3.2.

These inferences about Pb contamination in lunar samples have some important implications. The hand-picked, leached mineral fractions preserve the best representation of the true Pb composition inherent to the sample, whereas the mesostasis-rich Ilm and WR(R) fractions are fundamentally more susceptible to contamination derived from the surface of the Moon. Therefore, it is not reliable to depend solely upon whole rock samples to determine initial Pb compositions and source μ values, unless there is supporting evidence, in the form of a U–Pb or Pb–Pb age that is concordant with a Sm–Nd or Rb–Sr age, that the Pb isotope systematics of the whole rock are not disturbed. It is also important to note that there are many mechanisms by which Pb in a lunar sample may be disturbed, and therefore there is no single reliable test for disturbance—each sample must be evaluated on a case-by-case basis (e.g., Edmunson et al., 2006). It is only with Pb isotope data for multiple mineral fractions, accompanied by Rb–Sr or Sm–Nd data (preferably on those same mineral fractions), that the effects of disturbance to the Pb isotope systematics can be adequately evaluated. Therefore, in the following section, the petrogenetic discussion is restricted to samples for which the U–Pb or Pb–Pb isotope systematics reflect minimal post-crystallization disturbance, and for which reliable petrogenetic information can be obtained from the Pb isotope systematics.

5. LEAD ISOTOPE CONSTRAINTS ON THE ORIGIN OF GEOCHEMICAL DIVERSITY IN THE LUNAR MANTLE

The volatile and chalcophile nature of Pb means that the U–Pb isotope system can potentially record unique information about the geologic history of the Moon. Thus, the U–Pb isotope systematics of a variety of lunar sample suites can be used to constrain the controlling factors for a number of petrogenetic issues such as the degree of volatile depletion in the Moon as a result of the giant impact and the role of sulfides during lunar magma ocean crystallization. Here, we use our new results for 10017, as well as existing isotope data for other lunar samples, to discuss the insights gained from the Pb isotopic record and their contribution towards understanding the evolution of the Moon.

Much of the lunar petrologic and geochemical record is consistent with a magma ocean model for formation of lunar mantle sources. In this model, an early, global molten layer in the Moon progressively crystallizes, and forms petrologically and geochemically distinct components in the mantle and crust (e.g., Smith et al., 1970; Wood et al., 1970; Warren, 1985). The general crystallization sequence is olivine–orthopyroxene–clinopyroxene–plagioclase–ilmenite, and throughout this sequence crystallization is dominated by co-precipitation of multiple phases (e.g., Snyder et al., 1992; Shearer and Papike, 1999). The final crystallization product is KREEP, which forms during the latest stages of magma ocean solidification, and is highly enriched in incompatible elements (including K, REEs, P, U, and Th). Sinking of ilmenite-bearing cumulates due to density instabilities may generate some mixing between ilmenite-free cumulates, ilmenite-bearing cumulates and KREEP (e.g., Shearer and Papike, 1999; Elkins Tanton et al., 2002).

According to the standard magma ocean model, lunar rock suites are either magma ocean crystallization products or melts of these products. For example, plagioclase is thought to have floated during crystallization to form the ferroan anorthosites, whereas the early formed mafic cumulates (ol + opx + cpx) are thought to dominate the source of the low-Ti mare basalts, and the late-formed mafic cumulates (ilmenite-bearing) dominate the source of the high-Ti mare basalts. KREEP is a major component in the high-Mg suite magmas as well as the KREEP basalts, and is a minor component in some of the mare basalts (Snyder et al., 1992, 1994). The predicted elemental fractionation during silicate and ilmenite crystallization in the magma ocean is consistent with $^{87}Rb/^{86}Sr$, $^{147}Sm/^{144}Nd$, and $^{176}Lu/^{177}Hf$ ratios of mare basalt compositional endmembers (Nyquist et al., 1977, 1979; Unruh et al., 1984; Snyder et al., 1994; Beard et al., 1998). We now add observations of the U–Pb isotope system to the discussion on the characteristics and origin of mare basalt source heterogeneity.

In order to compare mare basalts to one another on the basis of their source compositions, we calculated long-term $^{238}U/^{204}Pb$ ratios of mare basalt source regions using previously published isotope data as well as our new results for 10017 (Fig. 8). Because the U–Pb isotope data for lunar samples presented in the literature records varying extents of disturbance, we used some criteria to filter the data and identify samples from the literature with the least disturbed U–Pb systematics. These criteria are: an Rb–Sr or Sm–Nd age has been obtained for the sample; U–Pb isotopic data have been measured on mineral separates; and either the U–Pb or Pb–Pb system records an age that is concordant with the Rb–Sr or Sm–Nd age. Samples for which only whole rock U–Pb data exist are not included, as whole rock analyses do not provide adequate information with which to evaluate Pb disturbance in the sample. There are only six mare basalts that meet all three criteria. Two additional mare basalts (15555, 71055) that have ^{238}U–^{206}Pb and ^{235}U–^{207}Pb ages that are concordant with each other, but that are ~300 Ma older than Rb–Sr or Sm–Nd ages, are also included in the discussion.

Parent–daughter ratios of basalt sources are calculated using the initial isotopic composition of the sample, the crystallization age of the sample (defined by either Rb–Sr or Sm–Nd isochrons), and a model history (one- or two-stages of isotope ingrowth) of the sample's source. The initial isotopic composition of the sample is determined directly from the isochron, and therefore represents the composition of the magma at the time of crystallization. This is taken to be the magma's 'source composition', and it reflects the cumulative geologic history of the sample's source, including any and all melting, mixing or crystallization events that may have occurred prior to

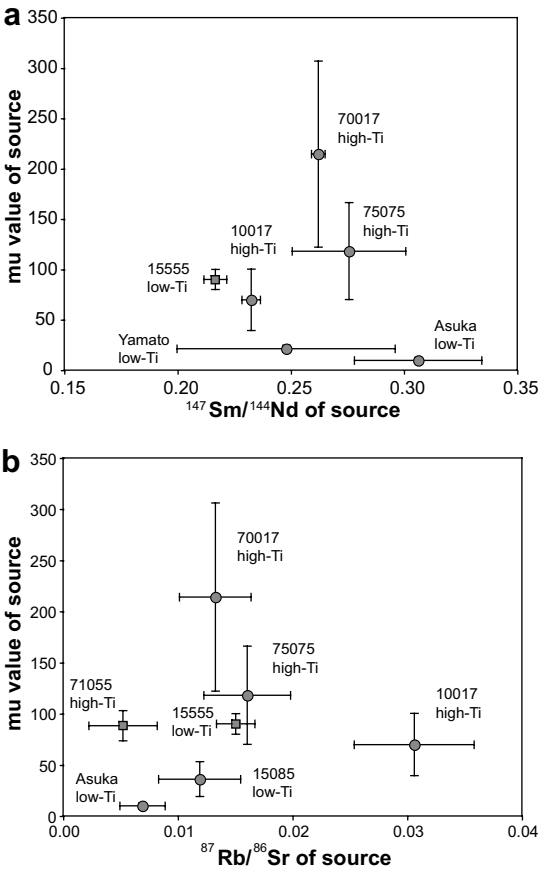

Fig. 8. $^{87}Rb/^{86}Sr$, $^{147}Sm/^{144}Nd$, and μ values calculated for mare basalt sources. See text for description of calculations. Samples shown with circle symbols have U–Pb and/or Pb–Pb age(s) that are concordant with Rb–Sr or Sm–Nd age. Samples shown with square symbols have ^{238}U–^{206}Pb and ^{235}U–^{207}Pb ages that are concordant with each other, but are ~300 Ma older than Rb–Sr or Sm–Nd ages. (Data sources: this study, Papanastassiou and Wasserburg, 1973; Tera and Wasserburg, 1974; Lugmair, 1975; Nyquist et al., 1975; Unruh and Tatsumoto, 1977; Chen et al., 1978; Unruh et al., 1984; Misawa et al., 1993; Torigoye-Kita et al., 1995).

crystallization of the basalt. Any constraints on the timing or mechanism of mixing among compositional end-members to form the 'source composition' specific to each sample are necessarily model-dependent, and our calculations make no attempt to place such constraints.

For the U–Pb system, the μ values of the basalt sources are calculated assuming single-stage growth in a reservoir with an initial Pb composition of Canyon Diablo Troilite (Tatsumoto et al., 1973; Chen and Wasserburg, 1983), from 4.558 Ga until the Rb–Sr or Sm–Nd crystallization age of the sample. For samples with ^{238}U–^{206}Pb and ^{235}U–^{207}Pb ages that are both concordant with Rb–Sr or Sm–Nd ages, both initial $^{206}Pb/^{204}Pb$ and initial $^{207}Pb/^{204}Pb$ are used to calculate the source μ values. The uncertainties associated with source μ values plotted for the various samples represent the range of source μ values that generate initial Pb compositions mutually consistent with Pb initials from both ^{238}U–^{206}Pb and ^{235}U–^{207}Pb isochrons. For samples with only one U–Pb age that is concordant with the Rb–Sr or Sm–Nd age, only the Pb initial from the concordant isochron is used to calculate the source μ value and uncertainty. If the source μ reported in the original publication includes evaluation of uncertainty, this is plotted as originally reported.

The μ values we calculate for the mare basalt source regions are generally much lower than values commonly estimated in other studies (see summary in Nyquist and Shih, 1992). However, our calculated μ values are still much higher than μ values of any other terrestrial planet, and thus the Moon retains its characteristic as the 'high-μ' terrestrial body. The 'low' mare basalt μ values presented here most likely reflect the fact that many of the previously published μ values for mare basalt sources are based upon whole rock analyses, which can lead to overestimations of initial Pb isotopic compositions. Lead isotope data from whole rock samples that have been contaminated by Pb derived from the lunar surface may yield high but spurious μ values for the mantle sources. For example, in the case of 15555, the original Pb isotope study reported a μ value of 240 for the mantle source (Tera and Wasserburg, 1974). Although some disturbance is evident in 15555, it is plausible that the total rock fraction shows effects of contamination by lunar Pb that are not evident in the plagioclase separate, and thus the source μ value based on the whole rock may be too high. Although our estimate of the initial Pb isotopic composition determined from the isochron may be too low, as the result of contamination of plagioclase and total rock fractions by terrestrial and lunar Pb, respectively, the true initial Pb composition and μ value of the source are probably lower than the values derived solely from the total rock analysis. For 15085, the original study (Unruh and Tatsumoto, 1977) also inferred a high μ value for the mantle source (~250–300). However, the U–Pb compositions of 15085 mineral and whole rock fractions do not appear to be significantly disturbed, and by using the initial Pb isotope ratios determined from U–Pb isochrons, we calculate a much lower μ value of ~35. Two mare basalt meteorites, Asuka-881757 and Yamato-793169, were recovered from Antarctica and thus may have become contaminated with terrestrial Pb during their residence in Antarctic ice. Asuka-881757 yields U–Pb ages that are concordant with Sm–Nd and Rb–Sr ages (Misawa et al., 1993). Therefore, any contamination is relatively minor, so this sample should give a reliable initial Pb composition and source μ values. Yamato-793169 shows some discrepancy among ages determined by various isotope systems, but the concordance of the ^{238}U–^{206}Pb age derived from all mineral fractions with the Sm–Nd age indicates that some initial Pb isotopic characteristics are preserved, and that the source μ value presented in this study is probably a good approximation of the actual value (Torigoye-Kita et al., 1995).

In Fig. 8, the calculated μ values of the mare basalt sources are compared to $^{87}Rb/^{86}Sr$ or $^{147}Sm/^{144}Nd$ compositions of the sources for these same samples. We calculate source parent–daughter ratios using initial $^{87}Sr/^{86}Sr$ and $^{143}Nd/^{144}Nd$ and crystallization ages determined from isochrons for as many samples as possible. For two of the samples shown in Fig. 8 (15555, 70017), only whole rock Sm–Nd isotope data exist, so we use these data, combined

with Rb–Sr crystallization ages, to determine the initial $^{143}Nd/^{144}Nd$. The calculations of source composition assume simple evolutionary histories of the source regions. The $^{147}Sm/^{144}Nd$ calculation assumes growth in a chondritic reservoir from 4.558 to 4.42 Ga (the KREEP model age, Nyquist and Shih, 1992), followed by growth from 4.42 to the time of eruption (t_i) in a source with $^{147}Sm/^{144}Nd$ that results in the initial $^{143}Nd/^{144}Nd$ determined from the isochron. The $^{87}Rb/^{86}Sr$ calculation uses a single-stage model with growth in a reservoir starting with the Sr isotopic composition of LUNI (LUNar Initial, Nyquist, 1977) at 4.558 Ga. For reference, most mare basalt sources have $^{147}Sm/^{144}Nd < 0.27$, and KREEP basalt sources have $^{147}Sm/^{144}Nd \geqslant 0.18$ (Nyquist and Shih, 1992; Snyder et al., 1995, 2000; Edmunson et al., 2005). Apollo 11, 12, and 17 collections each contain mare basalts that originate from sources with $^{147}Sm/^{144}Nd$ close to the upper bound of ~0.27, indicating that a depleted mare basalt source component is relatively widespread. Although these basalts originating from high-$^{147}Sm/^{144}Nd$ sources are also all high-Ti basalts, some high-Ti basalts are characterized by sources with lower $^{147}Sm/^{144}Nd$ values (Paces et al., 1991; Snyder et al., 1994; not shown in Fig. 8 because none of these samples have corresponding Pb data). Because the compilation of selected data includes so few samples, the range of source compositions shown in Fig. 8 cannot be considered to be truly representative on a global scale. Snyder et al. (1994, 1997) illustrate that $^{87}Rb/^{86}Sr$–$^{147}Sm/^{144}Nd$ variation among mare basalt sources requires heterogeneity greater than what can be described by only two components. The extent of this variation is not reflected by the samples shown in Fig. 8, and even on a very basic level there are no two samples that can be taken to represent compositional end-members in mare basalt sources.

The calculations summarized in Fig. 8 indicate that the mare basalt mantle sources have μ values that vary by at least an order of magnitude, despite the large uncertainties inherent to most lunar Pb isotopic data. This is an important observation that is not adequately explained in current models for the petrogenesis of mare basalt mantle sources. From the available data, it appears that there is no correlation between the μ value of the mantle source and either the $^{147}Sm/^{144}Nd$ or the $^{87}Rb/^{86}Sr$ of the source (Fig. 8). In fact, mantle sources with high μ values ($> \sim 75$) have $^{147}Sm/^{144}Nd$ and $^{87}Rb/^{86}Sr$ compositions that nearly span the range observed for all mare basalts. Furthermore, the most depleted mare basalt sources (based on highest $^{147}Sm/^{144}Nd$) have μ values that vary by an order of magnitude, whereas mare basalts from enriched sources (with low $^{147}Sm/^{144}Nd$) have moderate source μ values. Although this may, in part, reflect the limited nature of this subset of samples, it additionally may indicate that different geologic processes control U–Pb fractionation than those that control Rb–Sr and Sm–Nd fractionation in the mare basalt sources.

It has been shown that crystallization of silicate phases (olivine, orthopyroxene, clinopyroxene, plagioclase) and ilmenite, in the context of the magma ocean model, can generate the range in Rb/Sr, Sm/Nd, and Lu/Hf compositions determined for mare basalt source regions (Snyder et al., 1994; Beard et al., 1998). However, crystallization of these phases alone cannot generate the order-of-magnitude variation in μ values observed for lunar mantle sources. It is therefore necessary to call upon the involvement of some additional phase(s) or process(es) to generate large extents of U–Pb fractionation during magma ocean solidification. Furthermore, because μ is not correlated with $^{87}Rb/^{86}Sr$ or $^{147}Sm/^{144}Nd$ in mare basalt sources, the additional phase(s) or process(es) must have a minimal effect on these isotope ratios. Fractionation of sulfide minerals or an immiscible sulfide liquid in the late-stages of magma ocean crystallization may provide such a mechanism. Based on correlation of S with PGE contents in mare basalts, Neal et al. (2001) proposed that sulfide fractionation occurred during magma ocean crystallization. Lead is compatible in sulfide minerals, so sulfide fractionation generates remaining silicate melts with elevated U/Pb, which in turn imparts a high-μ signature on subsequently formed cumulates (Neal and Ely, 2002). Furthermore, varying extents of sulfide fractionation result in dramatic μ variability in residual liquids, and ultimately, late-stage KREEP with very high and possibly heterogeneous μ values.

Although currently there are not sufficient data to evaluate this model on a global level, we compare its first order predictions to the available observations. In this model, sulfide saturation occurs during the later-stages of the magma ocean crystallization sequence, after progressive crystallization of silicates (±ilmenite) has generated an increase in S concentrations in the remaining melt. Thus, ilmenite-free mafic cumulates, which formed early in the crystallization sequence, prior to or during the early stages of sulfide saturation, should have relatively low μ values. After sulfide saturation occurs, and sulfides or an immiscible sulfide liquid forms and sinks from the silicate portion of the system due to density differences, the μ value of the remaining silicate liquid progressively increases as sulfide continues to form and fractionate. Therefore, ilmenite-bearing cumulates, which formed later in the crystallization sequence, after sulfide began fractionating, should have higher μ values. Although there is not a distinct division between low-Ti and high-Ti basalts in terms of their μ values, the low-Ti basalts generally have μ values at the low end of the range observed in mare basalts and high-Ti basalts generally have μ values at the high end of the range.

Much of the U–Pb isotope record for other lunar samples is also broadly consistent with this scenario. Ferroan anorthosite 60025 is inferred to have formed from a low-μ source (16–55, Hanan and Tilton, 1987), which, together with the lunar meteorites (Misawa et al., 1993; Torigoye-Kita et al., 1995) and volcanic glasses (Tatsumoto et al., 1987) may closely represent the bulk μ of the moon (8–35, Premo et al., 1999). This indicates that the major lunar U–Pb fractionation occurred after plagioclase flotation in the lunar magma ocean as well as formation of the mantle sources of the low-μ basalts. Plagioclase crystallization probably increased U/Pb in the remaining liquid to some degree. However, we consider the later-stage sulfide fractionation was likely the primary process that generated order-of-magnitude variation in U/Pb ratios of the magma

ocean products, because the partition coefficient for Pb in sulfide is so much higher than for plagioclase. KREEP is the geochemical complement to magma ocean cumulates and formed last in the crystallization sequence. Thus, because it has experienced the greatest amount of sulfide fractionation, it is likely to have the highest μ values of any lunar source. Basalt and high-Mg suite samples enriched in KREEP have some of the highest μ values (>300–500) observed for lunar samples (Premo and Tatsumoto, 1991, 1992; Premo et al., 1999), consistent with the sulfide-fractionation scenario. This sulfide model carries the implication that there should exist a very low-μ, S-rich reservoir in the lunar mantle, or possibly the core. Such a reservoir is apparently not represented by any material in the current lunar sample suite.

The sulfide-fractionation model has specific implications for platinum group element (PGE) concentrations in the various geochemical reservoirs that form during magma ocean crystallization. However, PGEs have not been measured for most of the specific samples we discuss and no complete PGE sets have been measured for any of these samples. Thus, it is not possible to make any direct comparisons between calculated μ values of the mare basalt sources and PGE indices of sulfide fractionation. However, PGE measurements that are thought to represent pristine concentrations have been published for a few other mare basalts (e.g., Walker et al., 2004; Day et al., 2007). PGE patterns show greater variation for high-Ti basalts relative to the low-Ti basalts, which may reflect greater heterogeneity in the mantle source of the high-Ti mare basalts (Day et al., 2007). Furthermore, sulfur and PGE abundances and Pd/Ru and Pd/Rh ratios for low-Ti and some high-Ti mare basalts are consistent with sulfide fractionation during formation of the basalt sources (Neal et al., 2001; Neal and Ely, 2002). Mare basalts collected during the Apollo missions (both low- and high-Ti) have source μ values that are generally higher than the bulk moon μ value (8–35, Premo et al., 1999). This provides an additional indication that all of the mare basalts collected from the Apollo sites are derived from sources that experienced some degree of sulfide fractionation. However, the amount of sulfide fractionation that occurred prior to formation of the basalt sources varies among samples. For example, among the Apollo samples presented in Fig. 8, it appears that the source of one of the high-Ti basalts (70017) experienced the greatest amount of sulfide fractionation (and thus has the highest μ value), whereas the source of one of the low-Ti basalts (15085) experienced the least amount of sulfide fractionation (and thus has the lowest μ value). In contrast to the Apollo samples, the two meteorites have source μ values that are within the bulk moon range, and therefore are inferred to originate from sources that formed prior to sulfide fractionation. The simplest explanation for the combined observations from the existing PGE and Pb isotope data is that sulfide fractionation within the lunar magma ocean was heterogeneous on the scale of the different Apollo sampling sites, and that neither the Pb nor PGE data sets are extensive enough to completely represent the full extent of compositional variation in either μ value or PGE of the mare basalts and their mantle sources.

The relatively high μ value that historically has been inferred for the bulk moon (e.g., Unruh and Tatsumoto, 1977) contrasts with the low μ values inferred from this study as well as by Premo et al. (1999). This may reflect the fact that the Apollo collection is dominated by high-μ, KREEP-rich material. Although, KREEP is likely a volumetrically minor component of the Moon, impacts may have distributed KREEP-rich material, derived from the Procellarum KREEP Terrane (cf., Jolliff et al., 2000), over much of the lunar nearside. Soil that contains a component of KREEP-derived material will be characterized by radiogenic (ancient, high-μ) Pb, and is abundantly available as a contaminant of nearside lunar samples. Volatilization of Pb by impact also contributes to the re-distribution of this KREEP-derived radiogenic Pb.

It has long been recognized that the bulk μ value for the Moon is significantly larger than that for the Earth (~8–9). In contrast, the bulk μ value for Mars (~2–4, Chen and Wasserburg, 1986; Borg et al., 2005; Gaffney et al., 2006) is much lower than for either of these bodies. Although cores of different size and composition, which preferentially incorporate Pb relative to U, can explain some of the difference in bulk μ values of these planets, the relative abundances of volatile elements (Pb, Rb) is probably the dominant control on bulk planet Rb/Sr and U/Pb compositions. This is supported by the inverse correlation between estimates of bulk $^{87}Rb/^{86}Sr$ and $^{238}U/^{204}Pb$ for the Moon, Earth, and Mars.

6. CONCLUSIONS

Samarium–Nd, Rb–Sr, and ^{238}U–^{206}Pb isochrons yield concordant crystallization ages for mare basalt 10017 of 3.633 ± 0.057 Ga, 3.678 ± 0.069 Ga, and 3.616 ± 0.098 Ga, respectively. The ^{235}U–^{207}Pb isochron yields an older, though concordant, age of 3.80 ± 0.12. Neither the Pb–Pb isochron nor concordia system yields meaningful age information for 10017. The spread of the data in Pb–Pb space is consistent with contamination of the Ilm and WR(R) fractions by Pb with high $^{207}Pb/^{206}Pb$, derived from the lunar surface. However, this contamination did not have a dramatic effect on any of the other isochron systems. Consequently, we are able to determine initial Pb isotopic compositions from the U–Pb isochrons. These are: $^{206}Pb/^{204}Pb_i = 31 \pm 11$ and $^{207}Pb/^{204}Pb_i = 34 \pm 15$. The 10017 source μ value calculated assuming a single-stage of Pb growth and these initial Pb isotopic compositions, is 70 ± 30.

By using U–Pb isochrons in combination with Rb–Sr or Sm–Nd crystallization ages to evaluate the published U–Pb data sets for possible Pb disturbance, we find that the range of 'reliable' μ values for mare basalt sources is smaller and μ values are lower (10–215) than commonly inferred for mare basalt source regions (100–600). However, the order-of-magnitude variation in μ values of mare basalt sources appears to be characteristic. Calculated μ values of mare basalt sources do not correlate with $^{147}Sm/^{144}Nd$ or $^{87}Rb/^{86}Sr$, indicating that the U–Pb system reflects compositional heterogeneity that is not evident in these other isotope systems. This heterogeneity may reflect the involve-

ment of a phase or process during magma ocean crystallization that has minimal effect on Rb–Sr, Sm–Nd or Lu–Hf isotope relationships. Fractionation of sulfides or an immiscible sulfide liquid in which Pb is highly compatible is a mechanism that can produce both very high μ sources and large U–Pb fractionations during lunar magma ocean crystallization and formation of mare basalt mantle source regions. Generation of large variations in the μ values of lunar mantle source regions by sulfide crystallization in the lunar magma ocean is consistent with a much lower lunar bulk μ (8–35; Premo et al., 1999) than commonly estimated. The lunar bulk μ is higher than that for other terrestrial planets (~8–10, Earth; 2–4, Mars), and may be a fundamental reflection of the volatile-poor nature of the Moon relative to Earth or Mars.

ACKNOWLEDGMENTS

This paper benefited from constructive reviews by M. Anand, J. Day, and an anonymous reviewer. This work was supported by NASA-MFRP Grant NNG04GB32B and NASA-Cosmochemistry Grant NNG05GF83G to L.E.B. A portion of the work by A.M.G. and L.E.B. was performed under the auspices of the U.S. Department of Energy by the University of California, Lawrence Livermore National Laboratory under Contract No. W-7405-Eng-48.

REFERENCES

Apollo 11 Lunar Sample Catalogue (1977) Compiled by Kramer F. E., Twedell D. B., and Walton W. J. A. Jr. NASA Lyndon B. Johnson Space Center Publication JSC 12522, 478 pp.

Beard B. L., Taylor L. A., Scherer E. E., Johnson C. M., and Snyder G. A. (1998) The source region and melting mineralogy of high-titanium and low-titanium lunar basalts deduced from Lu–Hf isotope data. *Geochim. Cosmochim. Acta* **62**, 525–544.

Beaty D. W., and Albee A. L. (1978) Comparative petrology and possible genetic relations among the Apollo 11 basalts. In *Proc. 9th Lunar Planet. Sci. Conf.*, pp. 359–463.

Begemann F., Ludwig K. R., Lugmair G. W., Min K., Nyquist L. E., Patchett P. J., Renne P. R., Shih C. Y., Villa I. M., and Walker R. J. (2001) Call for an improved set of decay constants for geochronological use. *Geochim. Cosmochim. Acta* **65**, 111–121.

Borg L. E., Edmunson J. E., and Asmerom Y. (2005) Constraints on the U–Pb isotopic systematics of Mars inferred from a combined U–Pb, Rb–Sr, and Sm–Nd isotopic study of the Martian meteorite Zagami. *Geochim. Cosmochim. Acta* **69**, 5819–5830.

Borg L. E., Nyquist L. E., Taylor L. A., Wiesmann H., and Shih C.-Y. (1997) Constraints on Martian differentiation processes from Rb–Sr and Sm–Nd isotopic analyses of the basaltic shergottite QUE 94201. *Geochim. Cosmochim. Acta* **61**, 4915–4931.

Borg L. E., Nyquist L. E., Wiesmann H., Shih C.-Y., and Reese Y. (2003) The age of Dar al Gani 476 and the differentiation history of the martian meteorites inferred from their radiogenic isotopic systematics. *Geochim. Cosmochim. Acta* **67**, 3519–3536.

Chen J. H., Tilton G. R., Mattinson J. M., Vidal P. (1978) Lead isotope systematics of mare basalt 75075. In *Proc. 9th Lunar and Planet. Sci. Conf.*, pp. 509–521.

Chen J. H., and Wasserburg G. J. (1983) The least radiogenic Pb in iron meteorites. *Lunar Planet. Sci. Conf. XIV*, pp. 103–104 (abstr.).

Chen J. H., and Wasserburg G. J. (1986) Formation ages and evolution of Shergotty and its parent planet from U–Th–Pb systematics. *Geochim. Cosmochim. Acta* **50**, 955–968.

Curtis D. B., and Wasserburg G. J. (1975) Apollo 17 neutron stratigraphy—sedimentation and mixing in the lunar regolith. *The Moon* **13**, 185–227.

Day J. M. D., Pearson D. G., and Taylor L. A. (2007) Highly siderophile element constraints on accretion and differentiation of the Earth–Moon system. *Science* **315**, 217–219.

Dickinson T., Taylor G. J., Keil K., and Bild R. W. (1989) Germanium abundances in lunar basalts: evidence of mantle metasomatism? In *Proc. 19th Lunar and Planet. Sci. Conf.*, pp. 189–198.

Edmunson J., Borg L. E., Nyquist L. E., and Asmerom Y. (2005) Three-system isotopic study of lunar norite 78238: Rb–Sr results. *Lunar Planet. Sci. Conf. XXXIV*, #1473 (abstr.).

Edmunson J., Gaffney A. M., and Borg L. E. (2006) Disturbance of U–Pb isotopic systematics in lunar samples: mare basalt 10017 and norite 78238. *Lunar Planet. Sci. Conf. XXXVII*, #1506 (abstr.).

Elkins Tanton L. T., Van Orman J. A., Hager B. H., and Grove T. L. (2002) Re-examination of the lunar magma ocean cumulate overturn hypothesis: melting or mixing is required. *Earth Planet. Sci. Lett.* **196**, 239–249.

Fletcher I. R., and Rosman K. J. R. (1982) Precise determination of initial Nd from Sm–Nd isochron data. *Geochim. Cosmochim. Acta* **46**, 1983–1987.

Gaffney A. M., Borg L. E., and Connelly J. N. (2006) U–Pb isotope systematics of shergottite Queen Alexandra Range 94201: seeing through terrestrial lead contamination to identify an even lower-mu source on Mars. *Lunar Planet. Sci. Conf. XXXVII*, #1483 (abstr.).

Gopalan K., Kaushal S., Lee-Hu C., and Wetherill G. W. (1970) Rb–Sr and U, Th–Pb ages of lunar materials. *Geochim. Cosmochim. Acta Suppl.* **1**, 1195–1205.

Hanan B. B., and Tilton G. R. (1987) 60025—relict of primitive lunar crust? *Earth Planet. Sci. Lett.* **84**, 15–21.

Hidaka H., Ebihara M., and Yoneda S. (2000) Neutron capture effects on samarium, europium, and gadolinium in Apollo 15 deep drill-core samples. *Meteorit. Planet. Sci.* **35**, 581–590.

Jolliff B. L., Gillis J. J., Haskin L. A., Korotev R. L., and Wieczorek M. A. (2000) Major lunar crustal terranes: surface expressions and crust-mantle origins. *J. Geophys. Res.* **105**, 4197–4216.

Jolliff B. L., Haskin L. A., Colson R. O., and Wadhwa M. (1993) Partitioning in REE-saturating minerals: theory, experiment, and modelling of whitlockite, apatite, and evolution of lunar residual magmas. *Geochim. Cosmochim. Acta* **57**, 4069–4094.

Kleine T., Palme H., Mezger K., and Halliday A. N. (2005) Hf–W chronometry of lunar metals and the age and early differentiation of the Moon. *Science* **310**, 1671–1674.

Lingenfelter R. E., Canfield E. H., and Hampel V. E. (1972) The lunar neutron flux revisited. *Earth Planet. Sci. Lett.* **16**, 355.

Ludwig K. R. (2001) Isoplot/Ex rev. 2.49; A geochronological toolkit for Microsoft Excel. In *Berkeley Geochronology Center Special Publication No. 1a*.

Lugmair G. W. (1975) Sm–Nd systematics of some Apollo 17 basalts. *LPI Contrib.* **234**, 107–110.

Minster J. F., Birck J. L., and Allegre C. J. (1982) Absolute age of formation of chondrites studied by the ^{87}Rb–^{87}Sr method. *Nature* **300**, 414–419.

Misawa K., Tatsumoto M., Dalrymple G. B., and Yanai K. (1993) An extremely low U/Pb source in the Moon—U–Th–Pb, Sm–Nd, Rb–Sr, and $^{40}Ar/^{39}Ar$ isotopic systematics and age of lunar meteorite Asuka 881757. *Geochim. Cosmochim. Acta* **57**, 4687.

Neal C. R., and Ely J. C. (2002) Sulfide immiscibility in the lunar magma ocean: evidence for a primitive lunar lower mantle and the origin of high-μ mare basalts. *Lunar Planet. Sci. Conf. XXXIII*, #1821 (abstr.).

Neal C. R., Ely J. C., and Jain J. C. (2001) The siderophile element budget of the Moon: a reevaluation, part 2. *Lunar Planet. Sci. Conf. XXXII*, #1662 (abstr.).

Nyquist L. E. (1977) Lunar Rb–Sr chronology. *Phys. Chem. Earth* **10**, 103–142.

Nyquist L. E., Bansal B. M., and Wiesmann H. (1975) Rb–Sr ages and initial $^{87}Sr/^{86}Sr$ for Apollo 17 basalts and KREEP basalt 15386. *Lunar Planet. Inst. Conf. Abst.*, pp. 610–612.

Nyquist L. E., Bansal B. M., Wooden J. L., and Wiesmann H. (1977) Sr-isotopic constraints on the petrogenesis of Apollo 12 mare basalts. In *Proc. Lunar Sci. Conf. 8th*, pp. 1383–1415.

Nyquist L. E., Hörz F., Wiesmann H., Shih C.-Y., and Bansal B. (1987) Isotopic studies of shergottite chronology: I. effect of shock metamorphism on the Rb–Sr system. *Lunar Planet. Inst. Conf. Abst.*, pp. 732–733.

Nyquist L. E., and Shih C.-Y. (1992) The isotopic record of lunar volcanism. *Geochim. Cosmochim. Acta* **56**, 2213–2234.

Nyquist L. E., Shih C.-Y., Wooden J. L., Bansal B. M., and Wiesmann H. (1979) The Sr and Nd isotopic record of Apollo 12 basalts: implications for lunar geochemical evolution. In *Proc. Lunar Sci. Conf. 10th*, pp. 77–114.

Nyquist L. E., Wiesmann H., Bansal B., Shih C.-Y., Keith J. E., and Harper C. L. (1995) ^{146}Sm–^{142}Nd formation interval for the lunar mantle. *Geochim. Cosmochim. Acta* **59**, 2817–2837.

Paces J. B., Neal C. R., Taylor L. A., Nakai S. I., and Halliday A. N. (1991) A strontium and neodymium isotopic study of Apollo 17 high-Ti mare basalts—resolution of ages, evolution of magmas, and origins of source heterogeneities. *Geochim. Cosmochim. Acta* **55**, 2025–2043.

Papanastassiou D. A., and Wasserburg G. J. (1973) Rb–Sr ages and initial strontium in basalts from Apollo 15. *Earth Planet. Sci. Lett.* **17**, 324–337.

Papanastassiou D. A., Wasserburg G. J., and Burnett D. S. (1970) Rb–Sr ages of lunar rocks from the Sea of Tranquillity. *Earth Planet. Sci. Lett.* **8**, 1–19.

Papike J. J., Hodges F. N., Bence A. E., Cameron M., and Rhodes J. M. (1976) Mare basalts—crystal chemistry, mineralogy, and petrology. *Rev. Geophys. Space Phys.* **14**, 475–540.

Premo W. R., and Tatsumoto M. (1991) U–Th–Pb isotopic systematics of lunar norite 78235. In *Proc. Lunar Planet. Sci. Conf.*, vol. 21, pp. 89–100.

Premo W. R., and Tatsumoto M. (1992) U–Th–Pb, Rb–Sr, and Sm–Nd isotopic systematics of lunar troctolitic cumulate 76535: implications on the age and origin of this early lunar, deep-seated cumulate. *Proc. Lunar Planet. Sci.* **22**, 381–397.

Premo W. R., Tatsumoto M., Misawa K., Nakamura N., and Kita N. I. (1999) Pb-isotopic systematics of lunar highland rocks (>3.9 Ga); constraints on early lunar evolution. In *Planetary petrology and geochemistry; the Lawrence A Taylor 60th birthday volume* (eds. G. A. Snyder, C. R. Neal, and W. G. Ernst). Bellwether Publishing, pp. 207–240.

Russ, III, G. P., Burnett D. S., and Wasserburg G. J. (1972) Lunar neutron stratigraphy. *Earth Planet. Sci. Lett.* **15**, 172.

Schmitt H. H., Lofgren G., Swann G. A., and Simmons G. (1970) The Apollo 11 samples: introduction. *Geochim. Cosmochim. Acta Suppl.* **1**, 1–54.

Shearer C. K., and Papike J. J. (1999) Magmatic evolution of the Moon. *Am. Mineral.* **84**, 1469–1494.

Silver L. T. (1970) Uranium–thorium–lead isotopes in some Tranquility Base samples and their implications for lunar history. *Geochim. Cosmochim. Acta Suppl.* **1**, 1533–1574.

Smith J. V., Anderson A. T., Newton R. C., Olsen E. J., Crewe A. V., Isaacson M. S., Johnson D., and Wyllie P. J. (1970) Petrologic history of the moon inferred from petrography, mineralogy and petrogenesis of Apollo 11 rocks. *Geochim. Cosmochim. Acta Suppl.* **1**, 897.

Snyder G. A., Borg L. E., Nyquist L. E., and Taylor L. A. (2000) Chronology and isotopic constraints on lunar evolution. In*Origin of the earth and moon* (eds. R. M. Canup and K. Righter). University of Arizona Press, pp. 361–395.

Snyder G. A., Lee D.-C., Taylor L. A., Halliday A. N., and Jerde E. A. (1994) Evolution of the upper mantle of the Earth's Moon: Neodymium and strontium isotopic constraints from high-Ti mare basalts. *Geochim. Cosmochim. Acta* **58**, 4795–4808.

Snyder G. A., Neal C. R., Taylor L. A., and Halliday A. N. (1997) Anatexis of lunar cumulate mantle in time and space: Clues from trace-element, strontium, and neodymium isotopic chemistry of parental Apollo 12 basalts. *Geochim. Cosmochim. Acta* **61**, 2731–2747.

Snyder G. A., Taylor L. A., and Halliday A. N. (1995) Chronology and petrogenesis of the lunar highlands alkali suite: cumulates from KREEP basalt crystallization. *Geochim. Cosmochim. Acta* **59**, 1185–1203.

Snyder G. A., Taylor L. A., and Neal C. R. (1992) A chemical model for generating the sources of mare basalts - Combined equilibrium and fractional crystallization of the lunar magmasphere. *Geochim. Cosmochim. Acta* **56**, 3809–3823.

Stacey J. S., and Kramers J. D. (1975) Approximation of terrestrial lead isotope evolution by a two-stage model. *Earth Planet. Sci. Lett.* **26**, 207–221.

Tatsumoto M. (1970) Age of the moon: an isotopic study of U–Th–Pb systematics of Apollo 11 lunar samples-II. *Geochim. Cosmochim. Acta Suppl.* **1**, 1595.

Tatsumoto M., Knight R. J., and Allegre C. J. (1973) Time differences in the formation of meteorites as determined from the ratio of lead-207 to lead-206. *Science* **180**, 1279–1283.

Tatsumoto M., Premo W. R., and Unruh D. M. (1987) Origin of lead from green glass of Apollo 15426—a search for primitive lunar lead. *J. Geophys. Res.* **92**, 361–371.

Tera F., and Wasserburg G. J. (1972) U–Th–Pb analyses of soil from the Sea of Fertility. *Earth Planet. Sci. Lett.* **13**, 457.

Tera F., and Wasserburg G. J. (1974) U–Th–Pb systematics on lunar rocks and inferences about lunar evolution and the age of the moon. *Lunar Planet. Sci. Conf.*, 1571–1599.

Torigoye-Kita N., Misawa K., Dalrymple G. B., and Tatsumoto M. (1995) Further evidence for a low U/Pb source in the moon: U–Th–Pb, Sm–Nd, and Ar–Ar isotopic systematics of lunar meteorite Yamato-793169. *Geochim. Cosmochim. Acta* **59**, 2621–2632.

Unruh D. M., Stille P., Patchett P. J., and Tatsumoto M. (1984) Lu–Hf and Sm–Nd evolution in lunar mare basalts. *J. Geophys. Res. Suppl.* **89**, 459–477.

Unruh D. M., and Tatsumoto M. (1977) Evolution of mare basalts—the complexity of the U–Th–Pb system. *Lunar Planet. Sci. Conf.*, pp. 1673–1696.

Walker R. J., Horan M. F., Shearer C. K., and Papike J. J. (2004) Low abundances of highly siderophile elements in the lunar mantle: evidence for prolonged late accretion. *Earth Planet. Sci. Lett.* **224**, 399–413.

Warren P. H. (1985) The magma ocean concept and lunar evolution. *Annu. Rev. Earth Planet. Sci.* **13**, 201–240.

Wood J. A., Dickey, Jr., J. S., Marvin U. B., and Powell B. N. (1970) Lunar anorthosites and a geophysical model of the moon. *Geochim. Cosmochim. Acta Suppl.* **1**, 965.

Associate editor: Clive R. Neal